Pharmaceutical Sciences and Drug Design
ISSN: 3062-4428
2025, Volume 5, Page No: 377-389

Available online at: www.galaxypub.co/page/journals

Galaxy Publication

Galaxy Publication

Design, Synthesis, and Mechanistic Evaluation of U12 Derivatives as Potent Anti-Hepatoma Agents Targeting G0/G1 Cell Cycle Arrest and Apoptosis via PI3K/AKT/mTOR Pathway

Nadine Laurent[1]*, Marc Lefevre[2], Sophie Dubois[3], Alain Robert[1]

[1]Department of Drug Design, Faculty of Pharmacy, University of Montpellier, Montpellier, France.
[2]Department of Pharmaceutical Sciences, Faculty of Pharmacy, University of Geneva, Geneva, Switzerland.
[3]Department of Medicinal Chemistry, Faculty of Pharmacy, University of Vienna, Vienna, Austria.

***E-mail** ✉ nadine.laurent@gmail.com

Received: 16 August 2025; **Revised:** 28 November 2025; **Accepted:** 04 December 2025

ABSTRACT

Ursodeoxycholic acid (UDCA) is a well-established treatment for liver conditions, with its derivative, U12, showing notable anti-hepatoma effects in prior research. However, U12's low polarity and the requirement for high dosages pose challenges to its druglikeness. In this study, twelve new derivatives of U12 were synthesized using substitution, esterification, and amidation methods, aimed at improving its pharmacological properties. Testing of these derivatives on hepatoma cell lines (HepG2) revealed that compounds U12-I, U12a-d, and U12h exhibited superior cytotoxic effects compared to U12 itself. Among them, U12a showed the most potent activity against hepatocellular carcinoma. Mechanistic investigations demonstrated that U12a inhibited HepG2 cell proliferation by causing G0/G1 phase cell cycle arrest and by suppressing the PI3K/AKT/mTOR pathway. Moreover, U12a induced apoptosis in HepG2 cells through activation of the caspase signaling cascade. In vivo experiments confirmed that U12a significantly reduced tumor growth in HepG2-derived xenografts, without causing notable side effects. Consequently, U12a holds promise as a potential therapeutic agent for hepatocellular carcinoma.

Keywords: Anti-hepatoma activity, U12a, U12 derivatives, G0/G1 Cell

How to Cite This Article: Laurent N, Marc Lefevre M, Dubois S, Robert A. Design, Synthesis, and Mechanistic Evaluation of U12 Derivatives as Potent Anti-Hepatoma Agents Targeting G0/G1 Cell Cycle Arrest and Apoptosis via PI3K/AKT/mTOR Pathway. Pharm Sci Drug Des. 2025;5:377-89. https://doi.org/10.51847/1fsUbm6pYM

Introduction

Hepatocellular carcinoma (HCC) is one of the most aggressive and fatal cancers, marked by its high ability to metastasize and invade other tissues. According to the International Agency for Research on Cancer (IARC), more than 910,000 new HCC cases and 830,000 deaths due to liver cancer were reported worldwide in 2020 [1]. Liver cancer holds the third spot for cancer-related mortality. Key factors contributing to the development of HCC include cirrhosis, chronic hepatitis B and C infections, excessive alcohol intake, and obesity. The high rate of recurrence and metastasis leads to a grim outlook for many patients [2, 3]. As most cases are diagnosed at advanced stages, treatment options are often limited. Currently, sorafenib is the only FDA-approved first-line systemic therapy for advanced HCC, with regorafenib and nivolumab serving as second-line treatments after sorafenib failure [4-6]. This highlights the urgent need to discover new, effective therapies for HCC.

Ursodeoxycholic acid (UDCA), a bile acid with hydrophilic properties, is widely used as a safe and effective treatment for liver diseases, particularly primary biliary cirrhosis (PBC) and cholestatic liver disorders [7, 8]. In recent years, research has shown that UDCA provides hepatocyte protection and can induce apoptosis in human hepatocarcinoma cell lines (HepG2). Additionally, it has been demonstrated to block colon cancer formation and has been evaluated in clinical phase III trials for preventing colorectal adenoma recurrence [9-12]. UDCA is also known to alleviate gastrointestinal disorders in patients with various cancers, including those of the stomach,

colon, lungs, and liver [13]. Despite its proven benefits, UDCA requires large doses (500–1000 mg/day) to reach therapeutic efficacy, which can be limiting. As a result, researchers have turned to modifying UDCA's structure to generate derivatives with better therapeutic potential and lower dosage requirements. For example, NorUDCA (24-norursodeoxycholic acid), a derivative with a shortened side chain, has shown significant therapeutic effects in cholestatic Mdr2 (Abcb4) knockout mice [14-16]. Several UDCA derivatives, particularly those conjugated with amino acids via N-acyl bonds, have demonstrated strong anti-cancer properties against a range of human cancer cell lines [17, 18]. One such derivative, HS-1183, which is a UDCA-L-phenylalanine benzyl ester conjugate, exerts anti-cancer effects by inducing apoptosis in human breast and prostate cancer cells via a p53-independent pathway. Additionally, it prevents cell death in human cervical carcinoma by promoting NF-κB nuclear translocation and activating the JNK pathway. However, it is prone to cleavage by intestinal and hepatic enzymes [19-21]. Furthermore, introducing nitrogen heterocycles, such as piperazine and cinnamylpiperazinyl groups, has been shown to improve the cytotoxic properties of bile acid derivatives against cancer cells [22, 23]. In our previous research, we identified that U12, a derivative of UDCA, exhibited anti-hepatoma effects through mTOR/S6K1, cyclinD1/CDK2/4, and caspase-dependent apoptotic signaling pathways in hepatocellular carcinoma cells. Further in vivo investigations using a tumor xenograft mouse model revealed that U12 was more potent than UDCA in anti-tumor activity and exhibited fewer side effects compared to fluorouracil (5-Fu) [24]. However, U12's low polarity and high dosage requirements limited its druglikeness. Therefore, there is a critical need to develop more active UDCA derivatives with lower toxicity. In this study, UDCA was employed as the base compound to further explore modifications to U12, aiming to identify derivatives with stronger pharmacological effects and better-defined structure–activity relationships. It is known that introducing halogen atoms can enhance a compound's druglikeness [25], and incorporating nitrogen heterocycles has been proven to significantly improve the anti-tumor effects of bile acid derivatives [22, 23]. Here, we report the synthesis of twelve U12 derivatives in two series (A and B) through substitution, esterification, and amidation reactions **(Figure 1).** The A series consists of halogen-substituted derivatives, while the B series includes UDCA conjugates with nitrogen heterocycles, cyclopropane, or substituted benzene rings linked via an N-acetyl group. We investigated the synthesis, cytotoxic activities, apoptotic mechanisms, and structure–activity relationships of these derivatives.

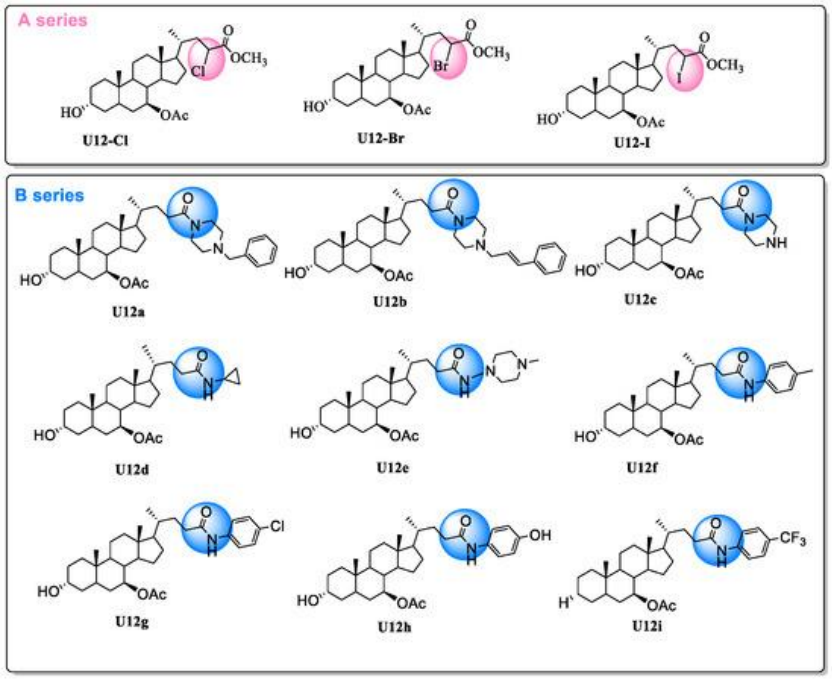

Figure 1. U12 derivatives of two series (A, B).

Materials and Methods

General experimental procedures

NMR analyses were performed on a Bruker Avance 600III (Bruker, Germany) spectrometer, using $CDCl_3$ as the solvent and tetramethylsilane (TMS) as the internal standard. High-resolution mass spectrometry (HR-ESI-MS) was conducted on a Thermo Scientific Q Exactive (Thermo, Waltham, MA, USA). Column chromatography was carried out using silica gel (200–300 mesh, Qingdao Marine Chemical Inc., China). For HPLC, a Shimadzu LC-20AT system (Shimadzu, Japan) equipped with a diode array detector (DAD) was used for analytical purposes, and preparative HPLC was performed on a Shimadzu LC-8A system (Shimadzu, Japan). Thin-layer chromatography (TLC) was employed to monitor reactions and was visualized under UV light (254 nm or 365 nm) after spraying with 5% sulfuric acid in ethanol, followed by heating. All reagents were sourced from commercial suppliers without further purification.

Synthesis procedures

Synthesis of 3α, 7β-diacetoxyursodeoxycholic acid (U-I)

UDCA (1.0 g, 2.55 mmol) was dissolved in ethyl acetate (100 mL) with 4-DMAP (100 mg, 0.8 mmol) and pyridine (10 mL). Acetic anhydride (12 mL) was then added dropwise, and the reaction was stirred at room temperature for 10 hours. The organic layer was extracted with water (100 mL) and ethyl acetate (100 mL). After washing with 1 M HCl and saturated NaCl solution, the combined organic extracts were dried over Na_2SO_4, concentrated under reduced pressure, and the resulting U-I was isolated as a colorless oil with a yield of 98%.

Synthesis of U12-Cl, U12-Br, and U12-I

U-I (200 mg, 0.42 mmol) was treated with $SOCl_2$ (5 mL), and the reaction was allowed to proceed at 40°C for 1 hour. The mixture was then heated to 70°C, and a bromine/pyridine/$SOCl_2$ mixture (55 μL/70 μL/400 μL) was added dropwise. After 6 hours of stirring, the solvent was evaporated under vacuum, and the residue was dissolved in CH_2Cl_2. Methanol was added dropwise at 4°C, and the mixture was concentrated to yield U12-Cl and U12-Br after HPLC purification. For U12-I, U12-Br (20 mg) was dissolved in acetone (2 mL), and NaI (5 mg) and $Bu_4N^+I^-$ (5 mg) were added. After stirring at room temperature for 6 hours, the mixture was extracted with water and ethyl acetate, dried over Na_2SO_4, and concentrated under vacuum to obtain U12-I.

Synthesis of U12a-U12i derivatives

To synthesize U12a-U12i derivatives, U-I (200 mg, 0.42 mmol) was dissolved in 10 mL of DMF under stirring. After the compound was fully dissolved, HOBt (30 mg, 2.21 mmol) and EDC•HCl (46 mg, 2.21 mmol) dissolved in DMF were added dropwise while maintaining a nitrogen atmosphere at 0°C. The reaction mixture was stirred for one hour, forming an intermediate product. Next, various amines such as benzylpiperazine, trans-1-cinnamylpiperazine, piperazine, cyclopropylamine, 1-amino-4-methylpiperazine, 4-aminotoluene, p-chloroaniline, 4-aminophenol, or 4-aminobenzotrifluoride (0.5 mmol) were added to the reaction, which was then left to react for another 24 hours. Afterward, the organic layer was extracted with water (50 mL) and ethyl acetate (50 mL). The solution was then dried using Na_2SO_4 and concentrated to yield crude products, which were purified by silica gel chromatography, obtaining U13a-U13i. The next step involved dissolving U13a-i (0.11 mmol) in THF (8 mL), followed by the addition of NaOH (16 mg, 0.4 mmol) dissolved in MeOH (1 mL). The mixture was stirred at room temperature for 1 hour, after which it was extracted with 1 M HCl (20 mL) and ethyl acetate (20 mL). The organic phase was washed with saturated NaCl solution (20 mL), dried over Na_2SO_4, and concentrated. The product was purified again using chromatography on silica gel to obtain U12a-U12i.

Characterization of final products

The final synthesized compounds (U-I, U12-Cl, U12-Br, U12-I, and U12a-U12i) were characterized using ^1H and ^{13}C NMR, as well as HR-ESI-MS.

MTT Assay for cell viability

Cell viability was assessed by performing the MTT assay. HepG2 cells were seeded in 96-well plates at a density of 1×10^4 cells per well and incubated overnight at 37°C in a 5% CO_2 atmosphere. The cells were then exposed to various compounds (U12 and its derivatives) at a final concentration of 25 μM for 24 hours. After treatment, the supernatants were discarded, and the cells were incubated with 75 μL of fresh medium and 15 μL of MTT solution for 4 hours. Following this, the MTT solution was removed, and the formed formazan crystals were

solubilized using 150 μL of DMSO. Absorbance was measured at 490 nm using a microplate reader. The viability was calculated using the following formula:

$$\text{Cell viability ratio (\%)} = (A_{treatment} - A_{blank})/(A_{control} - A_{blank}) \times 100\%. \quad (1)$$

Flow cytometry for cell cycle analysis

To analyze the effects of U12a on the cell cycle, HepG2 cells were cultured in 6-well plates and treated with varying concentrations of U12a (0, 6.25, 12.5, and 25 μM) for 24 hours. The cells were then trypsinized, washed with PBS, and fixed with 70% ethanol at 4°C overnight. After two washes with PBS, the cells were stained with RNase A (100 μL) and propidium iodide (400 μL) for 30 minutes at room temperature. The distribution of cells in different phases of the cell cycle (G1/G0, S, and G2/M) was analyzed using a BD FACS Calibur flow cytometer.

Annexin V-FITC/PI apoptosis assay

For apoptosis detection, HepG2 cells were seeded in 6-well plates at a density of 2×10^5 cells per well. After treatment with U12a at concentrations of 0, 6.25, 12.5, and 25 μM for 12 hours, the cells were harvested, resuspended in 1× binding buffer, and stained with 5 μL of Annexin V-FITC and 5 μL of propidium iodide. After incubation in the dark for 15 minutes, apoptosis was analyzed by flow cytometry within 1 hour.

Hoechst 33258 staining for nuclear morphology

HepG2 cells were seeded on 6-well plates at 1×10^5 cells/mL and incubated overnight. The cells were then treated with various concentrations of U12a (0, 6.25, 12.5, and 25 μM) for 24 hours. After treatment, the cells were harvested, washed with PBS, fixed with 4% formaldehyde, and stained with Hoechst 33258. The stained cells were visualized using fluorescence microscopy to observe any changes in nuclear morphology.

Western blotting for protein expression analysis

Western blotting was performed to determine the expression levels of specific proteins in HepG2 cells. The cells were lysed in SDS buffer, and protein concentrations were determined using the BCA protein assay. Equal amounts of protein were separated by SDS-PAGE and transferred onto PVDF membranes. After blocking, the membranes were incubated with primary antibodies for proteins such as mTOR, p-mTOR, p70S6k, p-p70S6k, Cyclin D1, Cdc25A, p27, CDK4, CDK6, and PARP. After incubation with the secondary antibody, the protein bands were detected using enhanced chemiluminescence and quantified using ImageJ software.

Evaluation of U12a's anti-tumor effects in the HepG2 xenograft model

Animal studies were performed following approval from the Institutional Animal Care and Use Committee at Xiamen University. Female nude mice (6 weeks old, BALB/c nu/nu) were sourced from Beijing Vital River Laboratory Animal Technology Co., Ltd. HepG2 cells (2.5×10^6 cells in 0.1 mL) were injected subcutaneously into the left flank of the mice to create a liver tumor model. Once the tumor volume reached approximately 200 mm^3 (around 8 days after injection), the mice were randomly divided into three groups: the control group (0.2% DMSO), the positive control (5-FU 30 mg/kg), and the experimental group (U12a 80 mg/kg). Treatment was given for 10 days, after which the mice were euthanized, and the tumors and liver tissues were collected. Tumors were fixed in formalin, processed, and analyzed for Ki-67 expression via immunostaining. Liver tissue from each group was examined using H&E staining. Tumor volumes were calculated using the formula:

$$\text{Volume } (mm^3) = 0.5 \times \text{length} \times \text{width}^2. \quad (2)$$

Statistical methods

The data are expressed as mean ± SD from three independent experiments. Statistical analysis was carried out using GraphPad Prism version 9.0 (GraphPad Software Inc., La Jolla, CA, USA). One-way ANOVA followed by Dunnett's test was applied to determine statistical significance, with a p-value of $p < 0.05$ considered significant.

Results and Discussion

Chemistry

The synthesis process began by acetylating UDCA (3α,7β-dihydroxycholanic acid) with acetic anhydride in ethyl acetate, using 4-dimethylaminopyridine (DMAP) as a catalyst, which resulted in the formation of the acetate derivative U-I. This intermediate U-I was then reacted with chlorosulfonyl chloride (SOCl2), followed by the addition of Br2 and pyridine, yielding a mixture of halogenated products. The reaction mixture was dissolved in dichloromethane (CH2Cl2) and added dropwise to cold methanol, which led to the formation of the chlorine (U12-Cl) and bromine (U12-Br) substituted derivatives. To produce U12-I, the U12-Br derivative was treated with sodium iodide (NaI) and tetrabutylammonium iodide (Bu4N+I−) in acetone, and the product was extracted with ethyl acetate.

In the next step, intermediate U-I underwent a reaction with 1-hydroxy benzotriazole (HOBt) and EDC•HCl (1-(3-dimethylaminopropyl)-3-ethylcarbodiimide hydrochloride) in N,N-dimethylformamide (DMF) under nitrogen atmosphere at low temperature (ice bath). The reaction mixture was then treated with various substituted piperazine derivatives, including benzylpiperazine (a), trans-1-cinnamylpiperazine (b), piperazine (c), cyclopropylamine (d), 1-amino-4-methylpiperazine (e), 4-aminotoluene (f), p-chloroaniline (g), 4-aminophenol (h), and 4-aminobenzotrifluoride (i), resulting in the formation of the corresponding carboxamide derivatives of U13 (U13a–U13i). Since U13 is the C-3 acetylated form of U12, the acetyl group in the U13 derivatives was hydrolyzed to a hydroxyl group using methanolic potassium hydroxide (KOH), yielding the deacetylated amides U12a–U12i **(Scheme 1).**

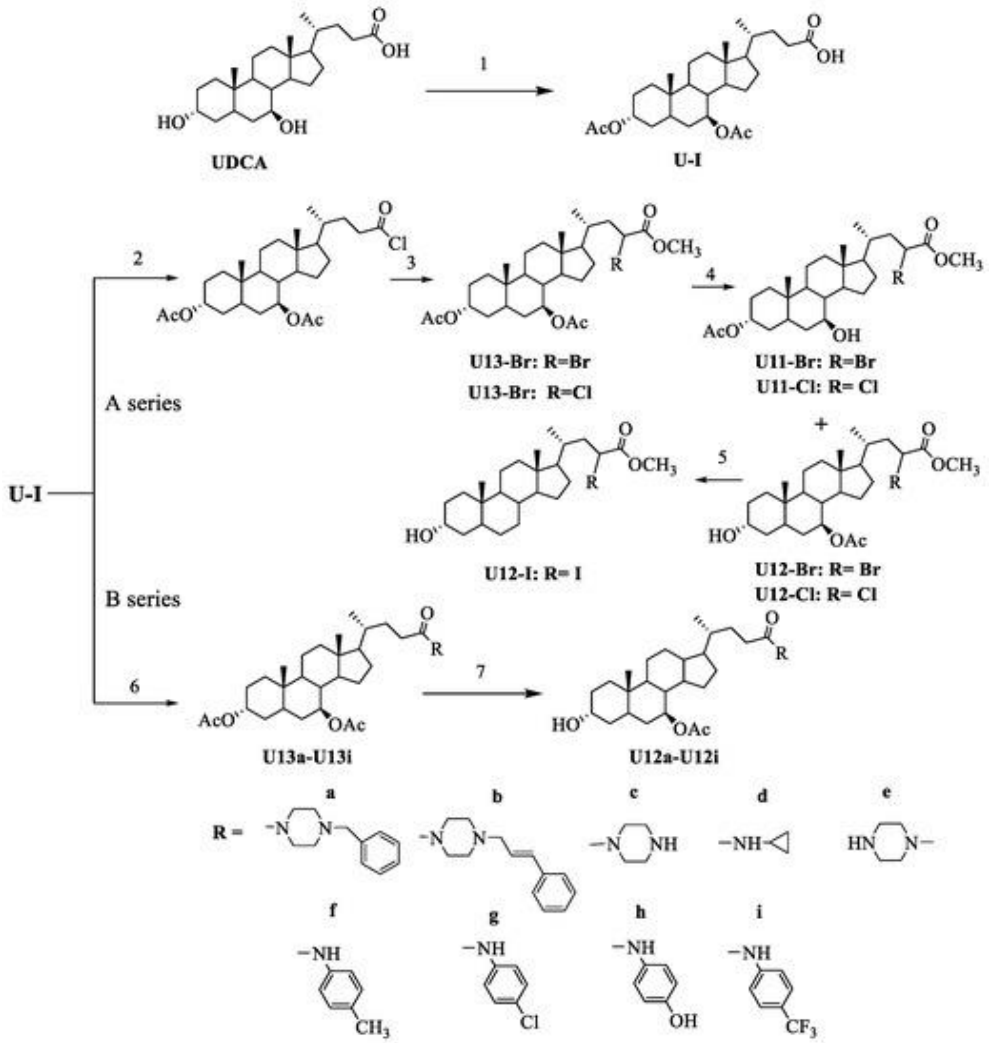

Scheme 1. Synthesis of U12 Derivatives. Conditions and Reagents:
(1) Ac2O, 4-DMAP, pyridine, room temperature (r.t.), 10 hours; (2) SOCl2, 40°C, 1 hour; (3) Br2, pyridine, SOCl2, 70°C, 6 hours; (4) CH2Cl2, methanol, 4°C; (5) NaI, Bu4N+I−, acetone, r.t., 6 hours; (6) HOBt, EDC•HCl, DMF, 4°C, 1 hour; a-i, 4°C, 24 hours; (7) NaOH, methanol, THF, r.t., 1 hour.**

The synthesized compounds were characterized using 1H NMR, HR-MS, and 13C NMR spectroscopy. For the halogen-substituted U12 derivatives (A series), the brominated derivative (Br-U12) was chosen as the example for structural determination. HR-ESI-MS analysis of Br-U12 confirmed the presence of a single bromine atom, with the isotope peak intensity ratio of 1:1 ([M+Na]+: [M+Na+2]+). In comparison with the 1D NMR data of U12, significant downshifts were observed for the chemical shifts of C-20, C-22, and C-23 in Br-U12 (δ 34.1, 40.7, and 45.7, respectively), indicating substitution of the H-23 group at the α-position of the carboxyl with a bromine atom.

For the B series (U12 conjugates), U12a was selected for detailed structural analysis. In addition to the typical steroid core signals of U12, the 13C NMR spectrum revealed additional peaks corresponding to the benzylpiperazine group: [δC 133.7 (C1, Ph), 129.3 × 2 (C3 and C5, Ph), 128.5 (C2 and C6, Ph), 127.5 (C4, Ph), 63.0 (C-Ph), 53.3 (CH2-, piperazinyl), and 52.9 (CH2-, piperazinyl)], which confirmed the formation of the piperazinylsteroid carboxamide. Moreover, HR-ESI-MS data of U12a provided the molecular formula C37H56O4N2, confirming the correct structure of U12a.

Biological Activities

Cytotoxicity of U12 derivatives on HepG2 cells

The cytotoxic effects of the synthesized U12 derivatives were assessed on HepG2 human hepatocellular carcinoma cells using MTT assays. The results showed that U12-I, U12a-d, and U12h were more cytotoxic than the parent compound U12 [24]. Among these, U12a exhibited the strongest cytotoxicity against HepG2 cells **(Figure 2a).** The cytotoxicity of U12a was further tested at various concentrations, showing a dose-dependent decrease in HepG2 cell viability across a concentration range of 0–25 μM, with an IC50 of 16.49 μM **(Figure 2b),** which was lower than U12, whose IC50 was above 25 μM. Additionally, the cytotoxicity of U12a and U12 was tested on two other hepatocellular carcinoma cell lines, Huh7 and SMMC-7721. U12a was found to be more effective in these two cell lines as well. Notably, the IC50 values for SMMC-7721 (>25 μM) and U12 against Huh7 (19.39 μM) were higher than that of HepG2 cells.

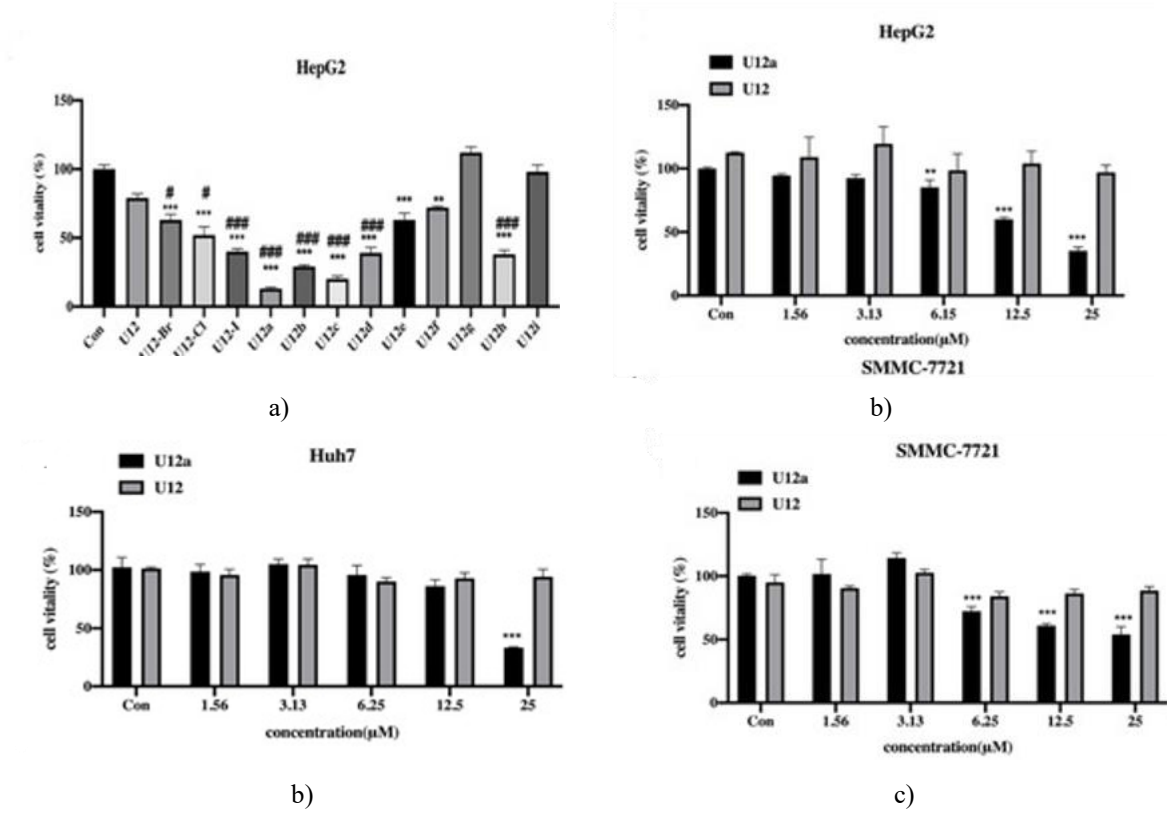

Figure 2. Cytotoxic Effects of U12 Derivatives on HepG2 Cells.
(a) Measurement of HepG2 cell viability following 24 hours of exposure to 25 μM of U12 derivatives, as assessed by MTT assay. (b–d) Impact of U12a and U12 on the viability of HepG2, Huh7, and SMMC-7721

cells, evaluated using MTT assay. HepG2 cells were treated with varying concentrations of U12a or U12 for 24 hours, followed by MTT staining, and the optical density (OD) was measured at 490 nm. Results are expressed as mean ± SD from three independent experiments. $p < 0.01$, *** $p < 0.001$ compared to control, # $p < 0.05$, ### $p < 0.001$ compared to U12 group.

The preliminary structure-activity analysis was performed. For the halogen-substituted derivatives (A series), the iodine-substituted U12-I at position C-23 demonstrated superior anti-hepatoma activity when compared to the bromine (U12-Br) and chlorine (U12-Cl) substituted derivatives. In the B series, the U12 derivatives U12a–U12c, which contain a piperazine group at position C-24, exhibited stronger anti-hepatoma activity than U12d–U12i, which feature -C(O)NH- linked functional groups. Among these, U12a, with a benzyl group attached, displayed the most potent cytotoxicity, surpassing U12c. Additionally, U12a showed greater cytotoxicity than U12b, suggesting that the cytotoxic effects diminish as the carbon chain linking the piperazine and benzene rings lengthens. Therefore, the piperazine ring at position C-24 is an essential active component, and the length of the carbon chain connecting the piperazine and the aromatic ring also plays a significant role in the compound's anti-hepatoma activity. U12d, with a -C(O)NH- linked cyclopropane group, was more potent than U12e, which had a -C(O)NH- linked methylpiperazine group, both showing improved cytotoxic effects compared to U12. Among the U12f–U12i derivatives, which incorporated -C(O)NH- linked benzene rings with various substituents like -CH3, -Cl, -OH, and -CF3, the cytotoxicity trend was: U12h (-OH) > U12f (-CH3) > U12i, U12g (-Cl, -CF3). This indicates that the presence of -C(O)NH- linked cyclopropane and phenol groups significantly boosts the cytotoxic activity of these derivatives.

U12a Inhibits HepG2 cell proliferation by blocking the G0/G1 phase

Uncontrolled proliferation is a hallmark of cancer. Inhibiting the cell cycle is an effective strategy to reduce cancer cell growth. The cell cycle is divided into several phases: G0/G1, S, G2, and M [26]. To determine whether U12a could induce cell cycle arrest in HepG2 cells, flow cytometry analysis was performed to assess the cell cycle distribution. As shown in **Figures 3a–3f**, treatment with U12a led to an accumulation of cells in the G0/G1 phase in a dose-dependent manner. In contrast, treatment with U12 (25 μM) did not induce cell cycle arrest **(Figures 3a–3f)**. Cyclin-dependent kinases (CDKs) and their cyclin partners form complexes that regulate the cell cycle [27]. When CDKs and cyclins are overexpressed, they can promote cancer cell apoptosis. Specifically, CDK4 and CDK6, in complex with cyclin D, control progression through the G1 phase, while the CDK2/cyclin E complex regulates the G1/S transition. The cell cycle regulator Cdc25A is frequently overexpressed in cancers and promotes cell cycle progression by activating CDKs. Cyclin kinase inhibitors (CKIs), including p21 and p27, can inhibit these complexes and control cell cycle progression, particularly at the G0/G1 transition [28, 29].

Based on the observed G0/G1 phase arrest caused by U12a, Western blotting was used to examine the expression of key cell cycle-related proteins. As shown in **Figures 3g and 3h**, treatment with U12a led to a dose-dependent decrease in the levels of Cdc25A, cyclin D1, CDK4, CDK6, cyclin E1, and CDK2. Additionally, U12a induced an increase in p21 levels, which is involved in G0-G1 regulation. In contrast, U12 (25 μM) did not alter the levels of any of these cell cycle proteins. Therefore, U12a inhibits HepG2 cell proliferation by causing G0/G1 phase arrest, while U12 has no effect at the same concentration.

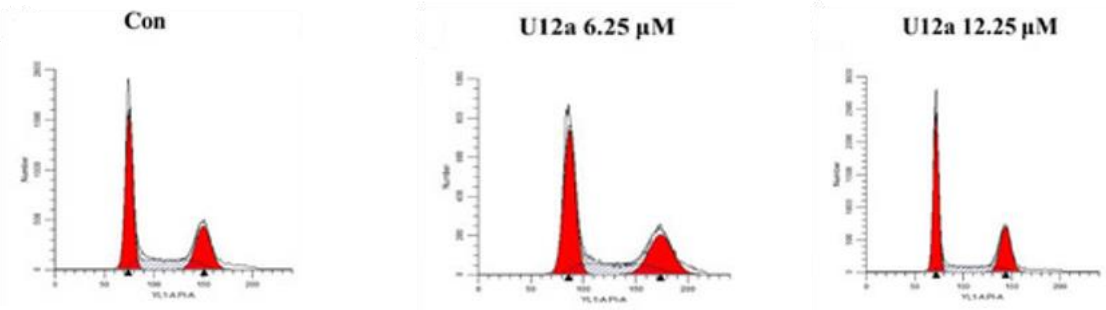

a) b) c)

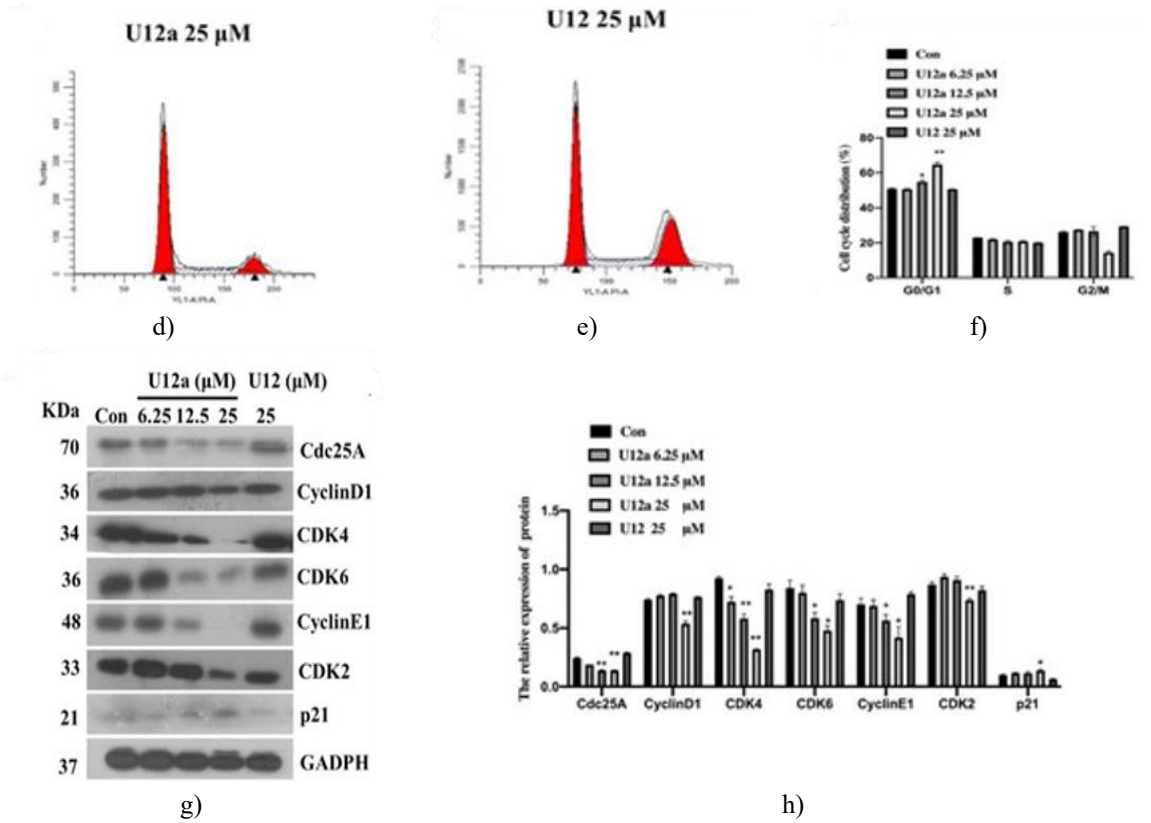

Figure 3. U12a Induces HepG2 Cell Cycle Arrest at G0/G1 Phase.
(a–f) HepG2 cells were exposed to U12a (6.25, 12.5, 25 μM) or U12 (25 μM) for 24 hours. Following treatment, cells were collected for flow cytometric analysis to assess cell cycle distribution. (g, h) Western blotting was used to analyze the expression levels of Cdc25A, Cyclin D1, CDK6, CDK4, Cyclin E1, p21, and p27. The results are presented as mean ± SD from three independent trials. * $p < 0.05$, ** $p < 0.01$ versus the untreated control group.

Pro-apoptotic action of U12a in HepG2 cells

Apoptosis is a programmed cell death process essential for removing abnormal or damaged cells [30]. To investigate whether U12a promotes apoptosis, flow cytometry with Annexin V-FITC/PI double staining was utilized. The data revealed a notable increase in apoptotic cells, from 13.0% in the control group to 14.8% (6.25 μM), 22.2% (12.5 μM), and 37.0% (25 μM) following 12 hours of U12a treatment **(Figures 4a–4f).** The apoptosis-inducing effect of U12a was further confirmed by Hoechst 33258 staining **(Figure 4g)**. Cleavage of poly (ADP-ribose) polymerase (PARP) serves as an important apoptosis marker. Western blot analysis showed that U12a treatment triggered a dose-dependent cleavage of PARP in HepG2 cells **(Figures 4h–4i).** In contrast, U12 (25 μM) did not induce PARP cleavage **(Figures 4a–4h).**

The caspase pathway is pivotal for apoptosis regulation. To explore if U12a activates caspase-dependent apoptosis, we measured the activities of caspases-3, -8, and -9 using specific assay kits. Caspase-3, the central executioner in apoptosis, is activated by the initiator caspases, -8 and -9. As shown in **Figure 4j**, the activities of caspases-3, -8, and -9 were all significantly elevated after treatment with U12a (25 μM) for 6 hours, with caspase-3 activity showing the most pronounced increase. These results suggest that U12a induces apoptosis in HepG2 cells by activating the caspase signaling cascade.

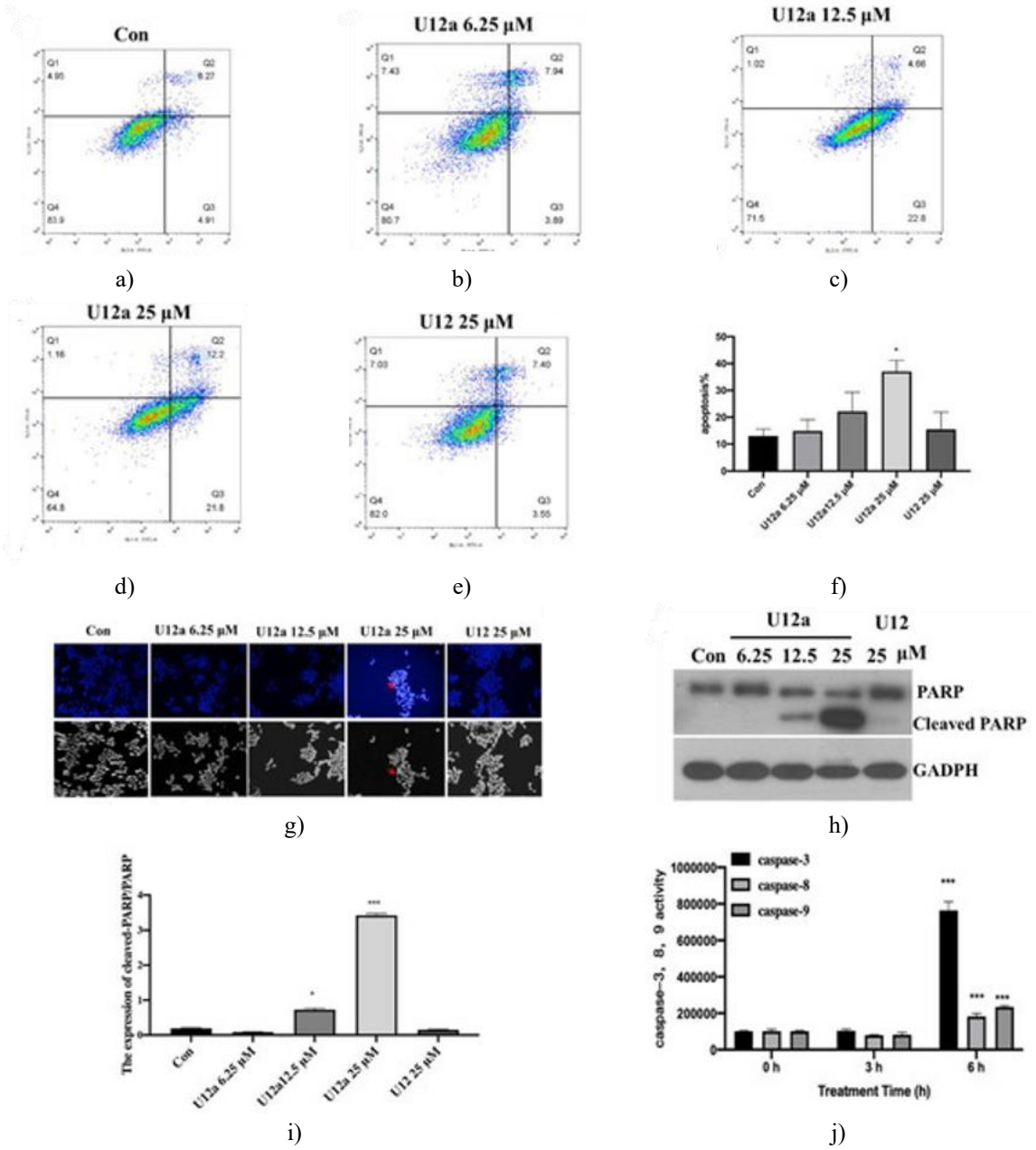

Figure 4. Apoptotic Effects of U12a on HepG2 Cells.

(a–f) The impact of U12a on HepG2 cell apoptosis was analyzed using Annexin V-FITC/PI double staining and flow cytometry. Cells were treated with varying concentrations of U12a (0, 6.25, 12.5, and 25 μM) and U12 (25 μM) for 12 hours. After staining with Annexin V FITC and propidium iodide, cells were analyzed for apoptosis. Early apoptotic cells were identified in the bottom right (E3), late apoptotic cells in the top right (E2), necrotic cells in the top left (E1), and healthy cells in the bottom left (E4). (g) Microscopic images were taken of HepG2 cells treated with U12a (6.25, 12.5, 25 μM) and U12 (25 μM) for 12 hours. Cell nuclei were stained with Hoechst 33528, and apoptotic cells were indicated by red arrows. (h, i) Western blot analysis revealed changes in the expression of PARP and cleaved PARP after treatment with U12a (6.25, 12.5, 25 μM) or U12 (25 μM) in HepG2 cells. (j) Caspase-3, -8, and -9 activities were measured using caspase kits following 6 hours of U12a (25 μM) exposure. * $p < 0.05$ vs. control group. *** $p < 0.001$ vs. control or 0-hour group.

U12a inhibits PI3K/AKT/mTOR signaling in HepG2 cells

The PI3K/AKT/mTOR pathway is essential for the development of hepatocellular carcinoma (HCC), with dysregulation observed in 40–50% of HCC cases [31]. To determine the effects of U12a on this pathway, HepG2 cells were treated with escalating doses of U12a for 24 hours. The results demonstrated a dose-dependent

inhibition of AKT and mTOR phosphorylation **(Figures 5a, and 4b).** Furthermore, mTOR activation influences the phosphorylation of p70S6k, a kinase that regulates cell growth. U12a was also found to suppress p70S6k phosphorylation in a concentration-dependent manner (**Figures 5a and 4b**). Collectively, these results suggest that U12a impedes the PI3K/AKT/mTOR signaling axis, ultimately restricting the proliferation of HepG2 cells.

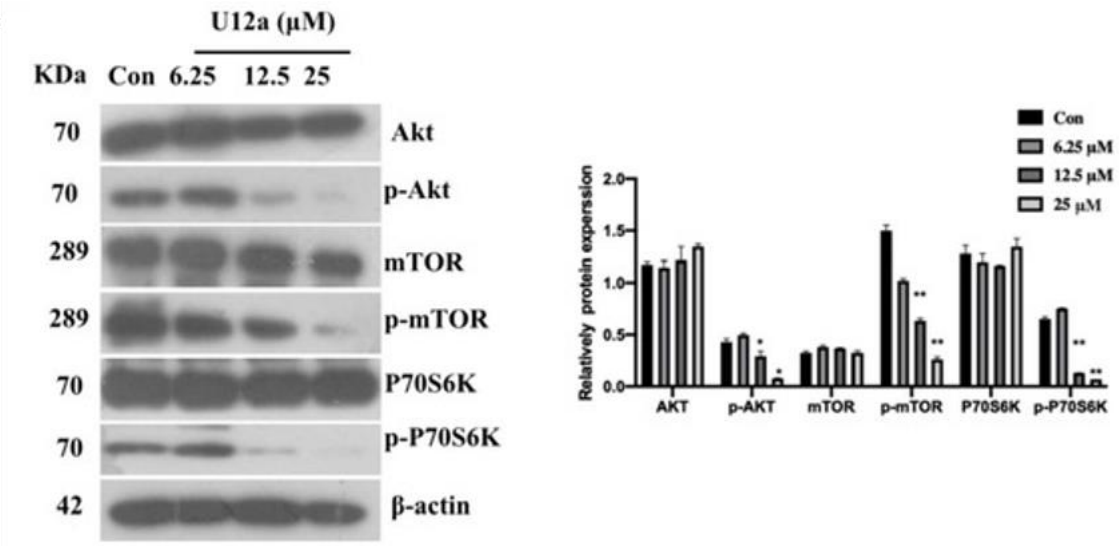

a) b)

Figure 5. Effect of U12a on the PI3K/AKT/mTOR Pathway in HepG2 Cells.
(a) The protein levels of AKT, p-AKT, mTOR, p-mTOR, p70S6k, p-p70S6k, and β-actin in HepG2 cells were measured after a 24-hour treatment with U12a at concentrations of 6.25, 12.5, and 25 μM. (b) The bar graph illustrates the relative intensity of the protein bands, as quantified using ImageJ. Data are expressed as the mean ± SD of three independent experiments. * $p < 0.05$, ** $p < 0.01$ compared to the control group.

Inhibition of tumor growth by U12a in the HepG2 xenograft model

In vitro experiments demonstrated that U12a significantly inhibited the proliferation of HepG2 cells. To assess its anti-cancer potential in vivo, a xenograft model in nude mice was used. Mice were given U12a through intraperitoneal injections at a dose of 80 mg/kg daily, with 5-FU (30 mg/kg) as a positive control. After 10 days of treatment, the animals were sacrificed, and the tumors were excised. As shown in **Figures 6a–6c**, U12a led to a marked reduction in tumor size compared to the control, with tumor growth inhibition comparable to 5-FU treatment. Additionally, U12a significantly decreased the Ki-67 expression, a well-known cell proliferation marker, in the tumor samples **(Figure 6d).** No significant weight loss was observed in the U12a-treated mice compared to the control group, both of which showed a slight weight increase, whereas the 5-FU group exhibited a noticeable decline in body weight due to side effects **(Figure 6e).** Further histopathological analysis of liver tissues, using H&E staining, showed no detectable abnormalities or damage in the U12a-treated group **(Figure 6f).** These findings suggest that U12a effectively inhibits tumor growth in vivo without causing significant toxicity.

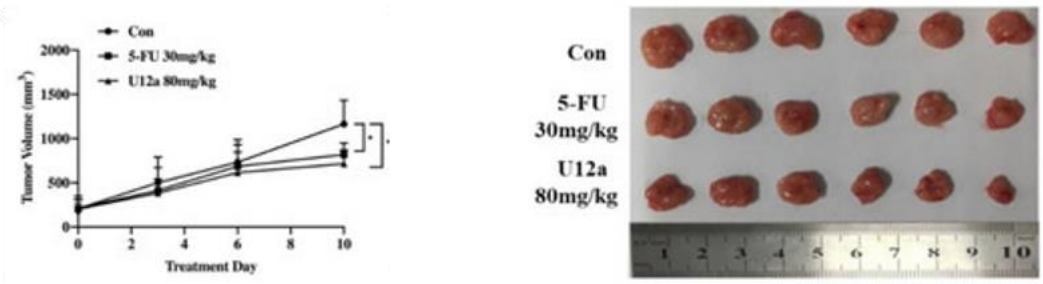

a) b)

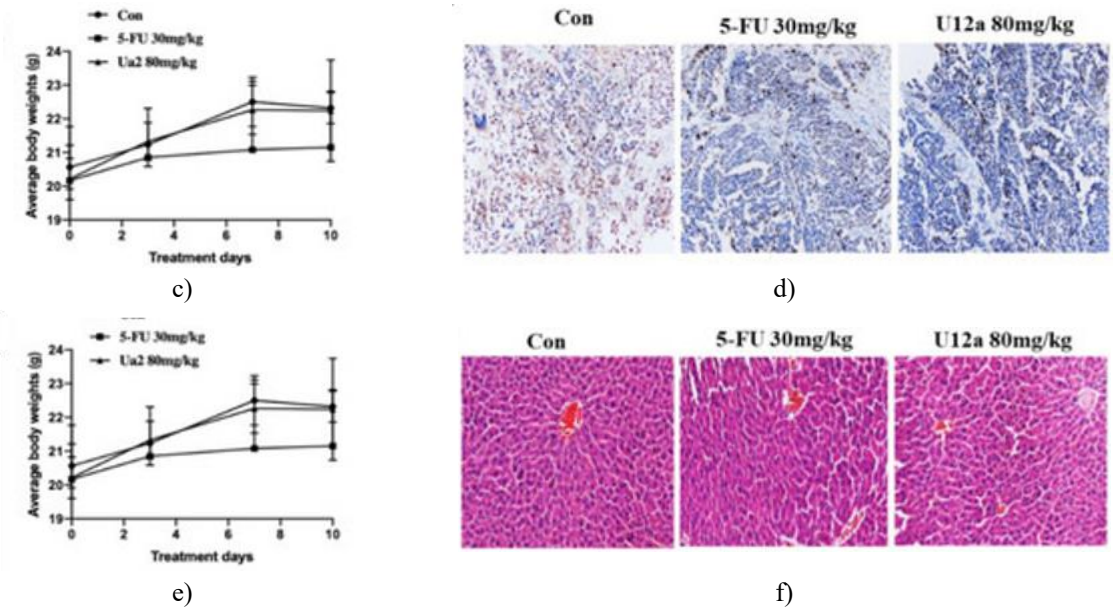

Figure 6. In vivo Evaluation of U12a in a Hepatocellular Carcinoma (HCC) Xenograft Model. (a) Tumor volume measurements across the different treatment groups (control, 5-FU at 30 mg/kg, U12a at 80 mg/kg). (b) Comparison of tumor size and weight in the groups. (c) Tumor weight comparison after treatment. (d) Immunohistochemical analysis of Ki-67, a marker of cellular proliferation, in excised tumors. (e) Monitoring the body weight of mice in each treatment group during the experiment. (F) H&E staining of liver tissues collected from the different groups. Values are represented as mean ± SD (n = 6). Statistical analysis shows significance: * $p < 0.05$, ** $p < 0.01$ compared to the control group.

Conclusion

UDCA is commonly used for treating cholestatic liver diseases. In a prior study, we identified that U12, a derivative of UDCA, demonstrated significant anti-hepatoma activity. However, its poor polarity and requirement for high dosages limited its clinical potential. To enhance its pharmacological profile, we synthesized a series of U12 derivatives through various chemical modifications. This study presents twelve U12 derivatives, divided into two groups (A and B), synthesized via halogen substitution, esterification, and amidation reactions. The A series consisted of halogen-substituted derivatives, and the B series included conjugates incorporating nitrogen-containing heterocycles, cyclopropane, or substituted aromatic rings attached to an N-acetyl group.

We assessed the synthesis, cytotoxic activity, apoptosis mechanisms, and structure–activity relationships of these derivatives. The testing on HepG2 cells revealed that most of the U12 derivatives, except for U12g and U12i, had superior cytotoxic effects compared to U12. Among them, U12a was the most potent against hepatocellular carcinoma. The structure–activity relationship suggests that the piperazine ring at position 24 plays a crucial role in the biological activity, and the length of the carbon chain linking the piperazine ring to the aromatic group also significantly impacts anti-hepatoma efficacy.

Mechanistic studies indicated that U12a inhibited HepG2 cell proliferation by causing a G0/G1 phase cell cycle arrest and also suppressed the PI3K/AKT/mTOR signaling pathway. Furthermore, U12a induced apoptosis in HepG2 cells through activation of the caspase signaling cascade. In vivo, U12a significantly reduced the growth of tumors in a HepG2 xenograft model without causing noticeable adverse effects. These findings suggest that U12a may be a promising candidate for treating hepatocellular carcinoma.

Acknowledgments: None

Conflict of Interest: None

Financial Support: None

Ethics Statement: None

References

1. Ferlay, J.; Colombet, M.; Soerjomataram, I.; Parkin, D.M.; Piñeros, M.; Znaor, A.; Bray, F. Cancer statistics for the year 2020: An overview. *Int. J. Cancer* 2021, *149*, 778–789.
2. Li, J.; Guo, W.; Xue, W.; Xu, P.; Deng, Z.; Zhang, D.; Zheng, S.; Qiu, X. Long noncoding RNA AURKAPS1 potentiates malignant hepatocellular carcinoma progression by regulating miR-142, miR-155 and miR-182. *Sci. Rep.* 2019, *9*, 19645.
3. Llopiz, D.; Ruiz, M.; Villanueva, L.; Iglesias, T.; Silva, L.; Egea, J.; Lasarte, J.J.; Pivette, P.; Trochon-Joseph, V.; Vasseur, B.; et al. Enhanced anti-tumor efficacy of checkpoint inhibitors in combination with the histone deacetylase inhibitor Belinostat in a murine hepatocellular carcinoma model. *Cancer Immunol. Immunother.* 2019, *3*, 379–393.
4. Llovet, J.M.; Ricci, S.; Mazzaferro, V.; Hilgard, P.; Gane, E.; Blanc, J.-F.; De Oliveira, A.C.; Santoro, A.; Raoul, J.-L.; Forner, A.; et al. Sorafenib in advanced hepatocellular carcinoma. *N. Engl. J. Med.* 2008, *359*, 378–390.
5. Bruix, J.; Qin, S.; Merle, P.; Granito, A.; Huang, Y.-H.; Bodoky, G.; Pracht, M.; Yokosuka, O.; Rosmorduc, O.; Breder, V.; et al. Regorafenib for patients with hepatocellular carcinoma who progressed on sorafenib treatment (RESORCE): A randomised, double-blind, placebo-controlled, phase 3 trial. *Lancet* 2017, *389*, 56–66.
6. Choi, W.M.; Choi, J.; Lee, D.; Shim, J.H.; Lim, Y.S.; Lee, H.C.; Kim, K.M.; Chung, Y.-H.; Lee, Y.S.; Park, S.R.; et al. Regorafenib Versus Nivolumab After Sorafenib Failure: Real-World Data in Patients With Hepatocellular Carcinoma. *Hepatol. Commun.* 2020, *4*, 1073–1086.
7. Lindor, K.D.; Gershwin, M.E.; Poupon, R.; Kaplan, M.; Bergasa, N.V.; Heathcote, E.J.; American Association for Study of Liver Diseases. Primary biliary cirrhosis. *Hepatology* 2009, *50*, 291–308.
8. Beuers, U.; Boyer, J.L.; Paumgartner, G. Ursodeoxycholic acid in cholestasis: Potential mechani- sms of action and therapeutic applications. *Hepatology* 2003, *28*, 1449–1453.
9. Park, I.H.; Kim, M.K.; Kim, S.U. Ursodeoxycholic acid prevents apoptosis of mouse sensory neurons induced by cisplatin by reducing P53 accumulation. *Biochem. Biophys. Res. Commun.* 2008, *377*, 1025–1030.
10. Khare, S.; Mustafi, R.; Cerda, S.; Yuan, W.; Jagadeeswaran, S.; Dougherty, U.; Tretiakova, M.; Samarel, A.; Cohen, G.; Wang, J.; et al. Ursodeoxycho -lic acid suppresses Cox-2 expression in colon cancer: Roles of Ras, p38, and CCAAT/enhancer-binding protein. *Nutr. Cancer* 2008, *60*, 389–400.
11. Alberts, D.S.; Martínez, M.E.; Hess, L.M.; Einspahr, J.G.; Green, S.B.; Bhattacharyya, A.K.; Guillen, J.; Krutzsch, M.; Batta, A.K.; Salen, G.; et al. Phoenix and Tucson Gastroenterologist Networks. Phase III trial of ursodeoxycholic acid to prevent colorectal adenoma recurrence. *J. Natl. Cancer Inst.* 2005, *97*, 846–853.
12. Centuori, S.M.; Martinez, J.D. Differential regulation of EGFR-MAPK signaling by deoxycholic acid (DCA) and ursodeoxy- cholic acid (UDCA) in colon cancer. *Dig. Dis. Sci.* 2014, *59*, 2367–2380.
13. Tatsumura, T.; Sato, H.; Yamamoto, K.; Ueyama, T. Ursodeoxycholic acid prevents gastrointestinal disorders caused by anticancer drugs. *Jpn. J. Surg.* 1981, *11*, 84–89.
14. Halilbasic, E.; Steinacher, D.; Trauner, M. Nor-Ursodeoxycholic Acid as a Novel Therapeutic Approach for Cholestatic and Metabolic Liver Diseases. *Dig. Dis.* 2017, *35*, 288–292.
15. Sombetzki, M.; Fuchs, C.D.; Fickert, P.; Österreicher, C.H.; Mueller, M.; Claudel, T.; Trauner, M.; Loebermann, M.; Engelmann, R.; Langner, C.; et al. 24-nor-ursodeoxycholic acid ameliorates inflammatory response and liver fibrosis in a murine model of hepatic schistosomiasis. *J. Hepatol.* 2015, *62*, 871–878.
16. Fickert, P.; Wagner, M.; Marschall, H.U.; Fuchsbichler, A.; Zollner, G.; Tsybrovskyy, O.; Zatloukal, K.; Liu, J.; Waalkes, M.P.; Cover, C.; et al. 24-norUrsodeoxycholic acid is superior to ursodeoxycholic acid in the treatment of sclerosing cholangitis in Mdr2 (Abcb4) knockout mice. *Gastroenterology* 2006, *130*, 465–481.
17. Berzigotti, A.; Bellot, P.; De Gottardi, A.; Garcia-Pagan, J.C.; Gagnon, C.; Spénard, J.; Bosch, J. NCX-1000, a nitric oxide-releasing derivative of UDCA, does not decrease portal pressure in patients with cirrhosis: Results of a randomized, double-blind, dose-escalating study. *Am. J. Gastroenterol.* 2010, *105*, 1094–1101.
18. Fiorucci, S.; Antonelli, E.; Brancaleone, V.; Sanpaolo, L.; Orlandi, S.; Distrutti, E.; Morelli, A.; Acuto, G.; Clerici, C.; Baldoni, M.; et al. NCX-1000, a nitric oxide-releasing derivative of ursodeoxycholic acid,

ameliorates portal hypertension and lowers norepinephrine-induced intrahepatic resistance in the isolated and perfused rat liver. *J. Hepatol.* 2003, *39*, 932–939.

19. Im, E.; Choi, S.H.; Suh, H.; Choi, Y.H.; Yoo, Y.H.; Kim, N.D. Synthetic bile acid derivatives induce apoptosis through a c-Jun N-terminal kinase and NF-kappaB-dependent process in human cervical carcinoma cells. *Cancer Lett.* 2005, *229*, 49–57.
20. Choi, Y.H.; Im, E.O.; Suh, H.; Jin, Y.; Yoo, Y.H.; Kim, N.D. Apoptosis and modulation of cell cycle control by synthetic derivatives of ursodeoxycholic acid and chenodeoxycholic acid in human prostate cancer cells. *Cancer Lett.* 2003, *199*, 157–167.
21. Im, E.O.; Choi, Y.H.; Paik, K.J.; Suh, H.; Jin, Y.; Kim, K.W.; Yoo, Y.H.; Kima, N.D. Novel bile acid derivatives induce apoptosis via a p53-independent pathway in human breast carcinoma cells. *Cancer Lett.* 2001, *163*, 83–93.
22. Brossard, D.; Lechevrel, M.; El Kihel, L.; Quesnelle, C.; Khalid, M.; Moslemi, S.; Reimund, J.M. Synthesis and biological evaluation of bile carboxamide derivatives with pro-apoptotic effect on human colon adenocarcinoma cell lines. *Eur. J. Med. Chem.* 2014, *30*, 279–290.
23. Brossard, D.; El Kihel, L.; Clément, M.; Sebbahi, W.; Khalid, M.; Roussakis, C.; Rault, S. Synthesis of bile acid derivatives and in vitro cytotoxic activity with pro-apoptotic process on multiple myeloma (KMS-11), glioblastoma multiforme (GBM), and colonic carcinoma(HCT-116) human cell lines. *Eur. J. Med. Chem.* 2010, *45*, 2912–2918.
24. Xu, Y.; Luo, Q.; Lin, T.; Zeng, Z.; Wang, G.; Zeng, D.; Ding, R.; Sun, C.; Zhang, X.; Chen, H. U12, a UDCA derivative, acts as an anti-hepatoma drug lead and inhibits the mTOR/S6K1 and cyclin/CDK complex pathways. *PLoS ONE* 2014, *9*, e113479.
25. Marcelo, Z.H.; Suellen, M.T.C.; Diogo, R.M.M.; Walter, F.D.A.J.; Ana, C.L.L. Halogen Atoms in the Modern Medicinal Chemistry: Hints for the Drug Design. *Curr. Drug Targets* 2010, *11*, 303–314.
26. Malumbres, M.; Barbacid, M. Cell cycle, CDKs and cancer: A changing paradigm. *Nat. Rev. Cancer* 2009, *9*, 153–166.
27. Besson, A.; Dowdy, S.F.; Roberts, J.M. CDK inhibitors: Cell cycle regulators and beyond. *Dev. Cell* 2008, *14*, 159–169.
28. Mou, Z.; Wang, Y.; Li, Y. Brazilein induces apoptosis and G1/G0 phase cell cycle arrest by up-regulation of miR-133a in human vestibular schwannoma cells. *Exp. Mol. Pathol.* 2019, *107*, 95–101.
29. Adhami, V.M.; Aziz, M.H.; Reagan-Shaw, S.R.; Nihal, M.; Mukhtar, H.; Ahmad, N. Sanguinarine causes cell cycle blockade and apoptosis of human prostate carcinoma cells via modulation of cyclin kinase inhibitor-cyclin-cyclin-dependent kinase machinery. *Mol. Cancer Ther.* 2004, *3*, 933–940.
30. Nikoletopoulou, V.; Markaki, M.; Palikaras, K.; Tavernarakis, N. Crosstalk between apoptosis, necrosis and autophagy. *Biochim. Biophys. Acta* 2013, *1833*, 3448–3459.
31. Sheng, X.; Zhu, P.; Zhao, Y.; Zhang, J.; Li, H.; Zhao, H.; Qin, J. Effect of PI3K/AKT/mTOR Signaling Pathway on Regulating and Controlling the Anti-Invasion and Metastasis of Hepatoma Cells by Bufalin. *Recent Pat. Anticancer Drug Discov.* 2021, *16*, 54–65.